Modeling and Optimization of Suspension SAN Polymerization Reactors

M. J. R. CAVALCANTI, J. C. PINTO

Programa de Engenharia Química/COPPE, Universidade Federal do Rio de Janeiro, Cidade Universitária, CP:68502, Rio de Janeiro 21945-970 RJ, Brazil

Received 3 October 1996; accepted 18 November 1996

ABSTRACT: A detailed mathematical model is developed to describe the operation of batch-modified SAN [styrene (ST)/acrylonitrile (AN)/α-methylstyrene (AMS)] terpolymerization reactors. The model is validated by comparing simulation results with published and plant experimental data. Optimal temperature policies and initiator feed concentrations are then computed. It is shown that optimal operation conditions may be extremely sensitive to small perturbations, so that optimal operation conditions may actually be unfeasible. It is also shown that average polymer molecular weight may be properly controlled by adding small amounts of inhibitor into the polymerization medium, which is usually cheaper than using chain transfer agents to control the average polymer molecular weight. © 1997 John Wiley & Sons, Inc. J Appl Polym Sci **65:** 1683–1701, 1997

Key words: SAN; polymerization; reactor; modeling; simulation; optimization

INTRODUCTION

SAN (styrene/acrylonitrile) copolymers are among the most popular thermoplastics due to their solvent resistance and improved tensile strength, when compared to polystyrene, finding applications in houseware (refrigerator shelves and drawers, coffee mugs), packaging (bottle closures and sprayers), furniture (chair backs and shells), electronics (battery cases, cassette parts), vehicles (internals), etc. About two hundred thousand metric tons of SAN copolymers and another two hundred thousand tons of modified SAN resins are produced every year in the world.[1] Most of the SAN is produced by either solution or suspension polymerizations in batch-stirred tank reactors. Therefore, developing operation policies for SAN reactors is of significant economic importance.

Compared to the literature available about other polymerization processes, such as emulsion, slurry, and bulk polymerizations, literature regarding suspension polymerization reactors is much more scarce. The field has been reviewed recently by Yuan, Kalfas, and Ray,[2] where it may be seen that most of the published articles are concerned with the proper description and control of particle size distributions, as the kinetics of suspension polymerizations is regarded to be similar to the kinetics of solution and bulk polymerizations, as monomer droplets may be seen as small bulk reactors that are suspended in a continuous phase. Detailed kinetic models were developed for styrene,[3] methyl methacrylate,[4] and vinyl chloride[5] homopolymerizations and SAN copolymerizations.[6] Kalfas and Ray[7] and Kalfas, Yuan, and Ray[8] developed a detailed kinetic model that was able to describe vinyl acetate homopolymerizations and styrene/methyl methacrylate copolymerizations successfully.

Few papers are available about SAN suspension polymerizations. Miyata and Makashio,[9] presented experimental data regarding the influence of the suspension agent concentration, agitation speed, and the organic/water feed ratio upon the final particle morphology. Belyaev, Kazanskaya,

Correspondence to: J. C. Pinto (pinto@peq.coppe.ufrj.br).

and Nikitina,[10] compared suspension SAN copolymers obtained when more than one initiator was used to catalyze the polymerization. They observed that the addition of a second initiator allowed the production of copolymers with larger average molecular weight. Xiuchun,[11] studied the influence of the suspension agent upon the terpolymerization of styrene/acrylonitrile/α-methylstyrene. As observed by Miyata and Makashio[9] and Xiuchun,[11] the influence of the suspension agent concentration, agitation speed, and organic/water feed ratio upon the kinetics of SAN copolymerization may be neglected.

The bulk SAN copolymerization was studied by Sebastian and Biesenberger,[12] Balaraman, Sarwade, and Nadkarni,[13] Garcia-Rubio et al.,[14] and Liu, Padias, and Hall.[15] Sebastian and Biesenberger[12] studied the thermal ignition of bulk SAN copolymerizations in the temperature range of 90–100°C. Balaraman, Sarwade, and Nadkarni,[13] analyzed the influence of water upon the bulk SAN copolymerization and only observed a small reduction of the overall reaction rate, without any significant change of the final polymer properties. Garcia-Rubio et al.[14] developed a very detailed study about the kinetics of bulk SAN copolymerization, specially regarding the gel effect, which causes the autoacceleration of the reaction rates. Liu, Padias, and Hall[15] studied the thermal SAN copolymerization and showed that acrylonitrile is not able to initiate the polymerization reaction spontaneously in the temperature range of 100–125°C.

Some additional works regarding the SAN copolymerization in other reaction systems are available. Hatate et al.[16,17] studied the SAN copolymerization in solutions of dimethyl formamide (DMF) and concluded that the classical Mayo–Lewis copolymerization model (or ultimate model) was not adequate to describe the experimental results obtained. Hendy[18] studied the semi-batch emulsion SAN copolymerization with controlled copolymer composition by manipulating the styrene feed rate. Kikuta and Omi[19] studied the influence of various operation parameters upon the SAN emulsion copolymerization. Lin, Chin, and Wang[20] studied the azeotropic SAN copolymerization in toluene at low monomer conversions. Sebastian and Biesenberger[21] studied the rate of decomposition of various initiators during SAN copolymerizations in DMF and showed that classical free-radical polymerization models were unable to reproduce experimental data. Dimonie et al.[22] and Djekhaba, Graillat, and Guillot[23] studied the emulsion SAN copolymerization at various water/organic feed ratios and showed that classical emulsion polymerization models were not able to reproduce experimental results in a broad range of operation conditions. Guillot[24,25] showed that reactivity ratios of emulsion SAN copolymerizations depend on temperature and on the water/organic feed ratio, and that they are different from the reactivity ratios evaluated in homogeneous SAN copolymerizations. The Ziegler–Natta SAN copolymerization was also studied by Deshpande et al.[26] and Gandhi, Sivaram, and Bhardwaj.[27]

Although some studies about the kinetics of AMS homopolymerization and styrene/AMS copolymerizations are available,[28–32] very little is known about the kinetics of AMS polymerizations in other systems. It seems that the only study available about the styrene/acrylonitrile/α-methylstyrene terpolymerization is presented by Xiuchun,[11] as already discussed, but detailed kinetic data are not presented. AMS rate constants are much smaller than styrene rate constants due to spatial limitations and it may be reasoned that, rather than modifying final polymer properties, AMS is usually added to SAN copolymerizations to improve reactor operation and control. It is known, however, that AMS may improve the thermal properties of the final polymer resin.

As shown in the previous paragraphs, modeling SAN copolymerization reactors may be quite difficult, due to the lack of data and, as observed in some cases, significant deviations from classical kinetics. It seems that the only attempt to model a suspension SAN copolymerization reactor was carried out by Hagberg,[6] who developed and implemented a mathematical model which, after being validated by actual plant data, was used to allow the choice of proper chain transfer agents (modifiers) and initiators for the production of specified resin grades. The model was constituted by the mass balance equations and thermodynamic equilibrium equations which describe the monomer partition between organic and aqueous phases. The method of moments was used to allow the computation of average polymer molecular weight. Garcia-Rubio et al.[14] developed a model to describe the bulk SAN copolymerization and allow the evaluation of certain parameters of the gel-effect correlation. Experimental monomer conversion data were used to validate the model.

Mathematical models are usually implemented to allow the improvement of process operation and control. As shown by Souza, Lima, and Pinto,[33] however, most optimization studies available for polymerization processes regard a small number

of systems and lack experimental validation. To our knowledge, detailed optimization studies of suspension polymerization reactors are not available in the open literature, although general discussions about process design and operation may be found.[4,34,35] Regarding the SAN copolymerization, Tirrel and Gromley[36] developed temperature programs for controlling copolymer composition in solution polymerizations. Tsoukas, Tirrel, and Stephanopoulos,[37] Farber,[38] Cawthon and Knaebel,[39] and Choi[40] studied multiobjective optimization techniques and developed optimal temperature and feed rate profiles to control polymer average molecular weight and polymer composition in semi-batch and continuous solution SAN polymerizations. Guillot[24,25] studied the optimum water/organic ratio in emulsion SAN polymerizations in order to produce constant composition polymers.

The main objective of this article is to present a detailed model for suspension-modified SAN batch terpolymerization reactors and to show that the model can describe available data reasonably well. Then the model is used to optimize the operation of an industrial reactor, by minimizing a cost function and manipulating temperature profiles and initial initiator and modifier compositions. An independent experimental evolutionary optimization procedure (EVOP) is used to reach the optimum operation point and very similar optimum conditions are reached, showing that the model describes the process operation very accurately. Then, based on simulation results, it is shown that optimum conditions are placed at the borders that separate unstable and stable operation and are very sensitive to small process changes. It is also shown that effective control of average polymer molecular weight may be attained by adding small amounts of inhibitor in the polymerization medium, which may contribute to the reduction of operation costs.

Table I Reaction Mechanism

Spontaneous thermal initiation of styrene	
$3\,M_1 \rightarrow 3\,P_{100}$	ks
Initiation by initiator decomposition	
$I_1 \rightarrow 2\,R^{\bullet}$	k_{D1}
$I_2 \rightarrow 2\,R^{\bullet}$	k_{D2}
$R^{\bullet} + M_1 \rightarrow P_{100}$	ki_1
$R^{\bullet} + M_2 \rightarrow Q_{010}$	ki_2
$R^{\bullet} + M_3 \rightarrow W_{001}$	ki_3
Propagation	
$P_{n,m,l} + M_1 \rightarrow P_{n+1,m,l}$	kp_{11}
$P_{n,m,l} + M_2 \rightarrow Q_{n,m+1,l}$	kp_{12}
$P_{n,m,l} + M_3 \rightarrow W_{n,m,l+1}$	kp_{13}
$Q_{n,m,l} + M_1 \rightarrow P_{n+1,m,l}$	kp_{21}
$Q_{n,m,l} + M_2 \rightarrow Q_{n,m+1,l}$	kp_{22}
$Q_{n,m,l} + M_3 \rightarrow W_{n,m,l+1}$	kp_{23}
$W_{n,m,l} + M_1 \rightarrow P_{n+1,m,l}$	kp_{31}
$W_{n,m,l} + M_2 \rightarrow Q_{n,m+1,l}$	kp_{32}
$W_{n,m,l} + M_3 \rightarrow W_{n,m,l+1}$	kp_{33}
Chain transfer to monomer	
$P_{n,m,l} + M_1 \rightarrow \Lambda_{n,m,l} + P_{100}$	kf_{11}
$P_{n,m,l} + M_2 \rightarrow \Lambda_{n,m,l} + Q_{010}$	kf_{12}
$P_{n,m,l} + M_3 \rightarrow \Lambda_{n,m,l} + W_{001}$	kf_{13}
$Q_{n,m,l} + M_1 \rightarrow \Lambda_{n,m,l} + P_{100}$	kf_{21}
$Q_{n,m,l} + M_2 \rightarrow \Lambda_{n,m,l} + Q_{010}$	kf_{22}
$Q_{n,m,l} + M_3 \rightarrow \Lambda_{n,m,l} + W_{001}$	kf_{23}
$W_{n,m,l} + M_1 \rightarrow \Lambda_{n,m,l} + P_{100}$	kf_{31}
$W_{n,m,l} + M_2 \rightarrow \Lambda_{n,m,l} + Q_{010}$	kf_{32}
$W_{n,m,l} + M_3 \rightarrow \Lambda_{n,m,l} + W_{001}$	kf_{33}
Chain transfer to chain transfer agent (modifier)	
$P_{n,m,l} + L \rightarrow \Lambda_{n,m,l} + X^{\bullet}$	kfl_1
$Q_{n,m,l} + L \rightarrow \Lambda_{n,m,l} + X^{\bullet}$	kfl_2
$W_{n,m,l} + L \rightarrow \Lambda_{n,m,l} + X^{\bullet}$	kfl_3
$X^{\bullet} + M_1 \rightarrow P_{100}$	kx_1
$X^{\bullet} + M_2 \rightarrow Q_{010}$	kx_2
$X^{\bullet} + M_3 \rightarrow W_{001}$	kx_3
Termination by combination	
$P_{n,m,l} + P_{r,q,z} \rightarrow \Lambda_{n+r,m+q,l+z}$	kc_{11}
$P_{n,m,l} + Q_{r,q,z} \rightarrow \Lambda_{n+r,m+q,l+z}$	kc_{12}
$P_{n,m,l} + W_{r,q,z} \rightarrow \Lambda_{n+r,m+q,l+z}$	kc_{13}
$Q_{n,m,l} + Q_{r,q,z} \rightarrow \Lambda_{n+r,m+q,l+z}$	kc_{22}
$Q_{n,m,l} + W_{r,q,z} \rightarrow \Lambda_{n+r,m+q,l+z}$	kc_{23}
$W_{n,m,l} + W_{r,q,z} \rightarrow \Lambda_{n+r,m+q,l+z}$	kc_{33}

MODELING

The suspension polymerization reactor modeled is a pressurized jacketed stirred tank reactor, which is assumed to be perfectly mixed. Reaction is initiated by lauroyl peroxide and takes place in suspended droplets, which contain styrene, acrylonitrile, and AMS in specified concentrations. The continuous phase contains water and dissolved reagents and is assumed to be in thermodynamic equilibrium with the organic phase. The vapor phase is assumed to be in equilibrium with both liquid phases.

Although the discussion presented in the previous section shows that penultimate effects may be important to describe SAN polymerizations, kinetic parameters for the penultimate model are not available in the literature. Thus, the more usual ultimate free-radical kinetic mechanism is used to describe the kinetics of SAN terpolymerization. The reaction mechanism is presented in Table I, while kinetic parameters are presented in Table II. It is important to emphasize that those

Table II Kinetic Parameters Used for Simulation

Parameter	Value (L gmol s)	Reference
ks	$2.19 \times 10^5 \exp(-19080/RT)$	Hui and Hamielec[47]
k_{D1}	$3.954 \times 10^{14} \exp(-29584/RT)$	Akzo Catalog
kp_{11}	$1.06 \times 10^7 \exp(-7067/RT)$	Tsoukas, Tirrel, and Stephanopoulos[37]
kp_{22}	$3.00 \times 10^7 \exp(-4100/RT)$	Tsoukas, Tirrel, and Stephanopoulos[37]
kp_{33}	$0.15\ kp_{11}$	Rudin and Chiang[31]
r_{12}	$2.56 \exp(-1190/RT)$	Tsoukas, Tirrel, and Stephanopoulos[37]
r_{13}	1.12	Brandrup and Imemrgut[46]
r_{21}	$6.67 \times 10^{-5} \exp(4310/RT)$	Tsoukas, Tirrel, and Stephanopoulos[37]
r_{23}	0.04	Brandrup and Immergut[46]
r_{31}	0.63	Brandrup and Immergut[46]
r_{32}	0.10	Brandrup and Immergut[46]
kf_{11}	$2.31 \times 10^6 \exp(-12670/RT)$	Tsoukas, Tirrel, and Stephanopoulos[37]
kf_{22}	$6.93 \times 10^6 \exp(-5837/RT)$	Tsoukas, Tirrel, and Stephanopoulos[37]
kf_{33}	$0.15\ kf_{11}$	Note 1[a]
kf_{12}	$30\ kf_{11}$	Tsoukas, Tirrel, and Stephanopoulos[37]
kf_{13}	$kf_{12}\ (kp_{13}/kp_{12})$	Note 2
kf_{21}	$5\ kf_{22}$	Tsoukas, Tirrel, and Stephanopoulos[37]
kf_{23}	$kf_{21}\ (kp_{23}/kp_{21})$	Note 2[b]
kf_{31}	$kf_{11}\ (kf_{31}/kp_{11})$	Note 2
kf_{32}	$kf_{12}\ (kp_{32}/kp_{12})$	Note 2
kfl_1	$kf_{11}/3.2$	Elf-Atochem Catalog
kfl_2	$kf_{22}/0.18$	Elf-Atochem Catalog
kfl_3	$kf_{33}/3.2$	Note 1
kc_{11}	$1.25 \times 10^9 \exp(-1677/RT)$	Tsoukas, Tirrel, and Stephanopoulos[37]
kc_{22}	$3.3 \times 10^{12} \exp(-5400/RT)$	Tsoukas, Tirrel, and Stephanopoulos[37]
kc_{33}	kc_{11}	Note 1
kc_{12}	$[\varphi_{12} \sqrt{kc_{11}\ kc_{22}}]$	Definition
kc_{13}	$[\varphi_{13} \sqrt{kc_{11}\ kc_{33}}]$	Definition
kc_{23}	$[\varphi_{23} \sqrt{kc_{22}\ kc_{33}}]$	Definition
φ_{12}	23	Tsoukas, Tirrel, and Stephanopoulos[37]
φ_{13}	1	Rudin and Chiang[31]
φ_{23}	23	Note 1

[a] Note 1: Extending results presented by Rudin and Chiang[31] for propagation and termination of styrene/AMS copolymerizaiton at 60°C.
[b] Note 2: Assuming that transfer rates are proportional to rates of propagation.

parameters were collected from the open literature, at conditions which were similar to actual operation conditions, and were not subject to parameter estimation.

The mathematical model developed comprises the global mass balances of the chemical species, the energy balance, the thermodynamic equilibrium equations, and the momentum balances, obtained by averaging the mass balances of live and dead polymer chains of all sizes and used to describe the polymer average molecular weight and polydispersity. Model equations are presented in the Appendix. The resulting set of differential algebraic equations (DAE) was solved numerically

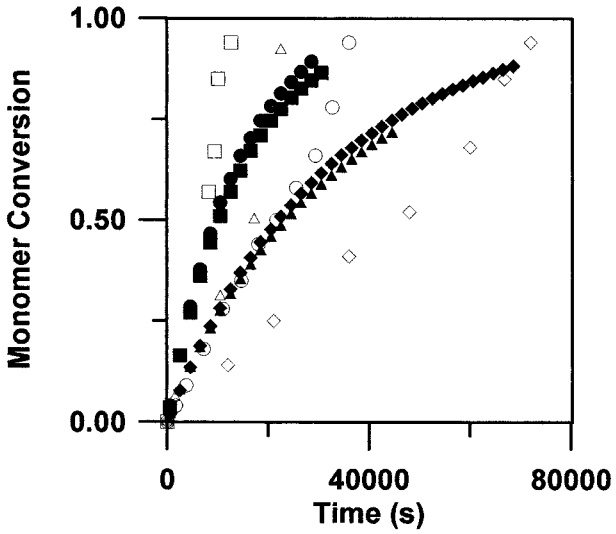

Figure 1 Conversion profiles for bulk SAN copolymerization at 60°C. Experimental data presented by Garcia-Rubio et al.[14] Simulations do not take the gel effect into account. Empty symbols are experimental results. Full symbols are simulation results. Numbers are initial styrene molar fraction and initiator concentration. (♦) 0.50, 0.01; (●) 0.50, 0.05; (▲) 0.90, 0.01; (■) 0.90, 0.05.

with the help of the computer code DDASSL,[41] which uses a BDF (backward differentiation formula) method to discretize and integrate the DAE system.

Model Validation

Figure 1 shows a comparison between simulation results and experimental results presented by Garcia-Rubio et al.[14] for bulk SAN copolymerization. Differences are due to the gel effect, which is the autoacceleration of monomer consumption caused by a decrease of the termination rates due to diffusion limitations in solutions with high polymer concentrations. The only available studies about the gel effect in SAN copolymerizations are those presented by Garcia-Rubio et al., who developed kinetic expressions for the gel effect based on the Free Volume Theory, but who took into account a different set of kinetic parameters, which are not able to reproduce actual plant data.[42] For this reason, it was decided to estimate the gel effect correlation, using data provided by Garcia-Rubio et al., and the parameters presented in Table II. Different empirical expressions presented by different authors were used as trial functions,[42] but the best results were obtained with the equations presented by Garcia-Rubio et al. The gel effect correlations are presented in the Appendix, where it is also shown that the parameters estimated for the gel effect correlations are extremely similar to those presented by Garcia-Rubio et al., showing that the kinetic parameters presented in Table II are also adequate to reproduce their experimental data. Figure 2 shows a comparison between simulation and experimental results.

The model was then used to simulate actual industrial operation conditions of a batch reactor. Detailed information about recipe formulation

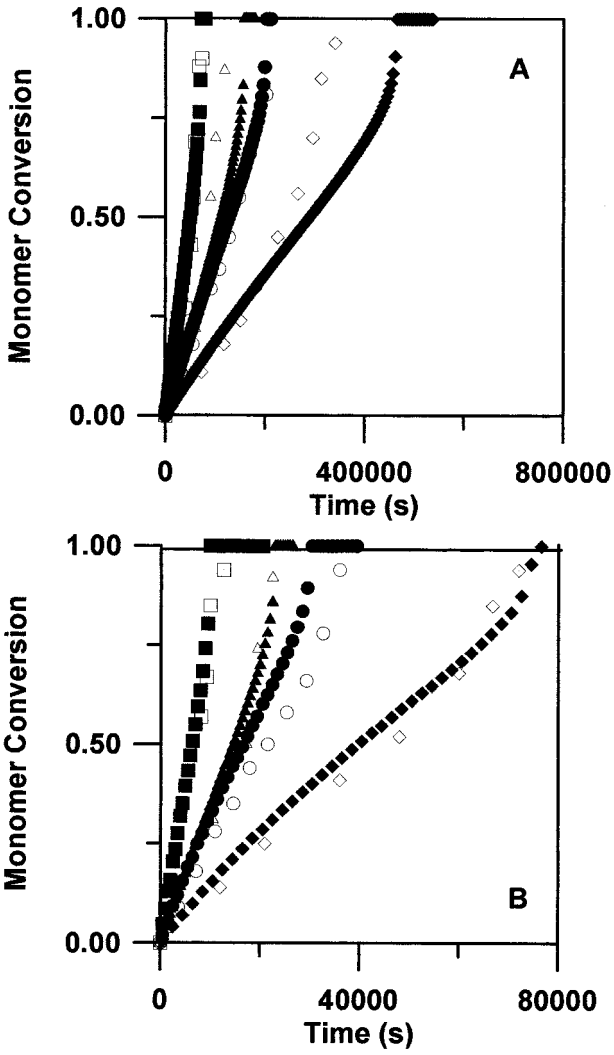

Figure 2 Conversion profiles for bulk SAN copolymerization. (A) 40°C, (B) 60°C. Experimental data presented by Garcia-Rubio et al.[14] Simulations take the gel effect into account. Empty symbols are experimental results. Full symbols are simulation results. Numbers are initial styrene molar fraction and initiator concentration. (♦) 0.50, 0.01; (●) 0.50, 0.05; (▲) 0.90, 0.01; (■) 0.90, 0.05.

Table III Dimensionless Operation Conditions

Chemical Species	Amount[a]
Styrene	69.3
Acrylonitrile	27.2
AMS	3.5
Initiator	1.5
Others	1.0
Water	93.0

[a] Parts per kilogram of monomer feed.

and reactor geometry cannot be presented due to proprietary reasons. However, it takes 2.5 h for a reaction to be finished and reactor temperature grows in an approximately linear form from 50 to 120°C. Table III presents the recipe formulation in dimensionless form. Heat transfer coefficients were obtained with independent heat transfer experiments. During the run, it is possible to take samples from the reactor to analyze polymer properties. Individual monomer conversion cannot be evaluated at the plant site, but reaction rates can be monitored by pressure measurements.

Figure 3 shows a comparison between experimental and simulation results obtained and it may be seen that they are in excellent agreement. It is interesting to observe that pressure grows fast at the end of the run and that the polymer composition is approximately constant throughout the run, indicating that the model is able to reproduce nearly azeotropic conditions. It is also important to observe that average polymer molecular weight decreases steadily with time and it is believed that the long polymer chains that are produced in the beginning of the run may be responsible for the appearance of "fish-eye" problems.

One possible way to avoid the production of long chains in the beginning of the run is to stop reaction during the first stages of the batch by adding small amounts of inhibitors to the reaction environment. By preventing polymerization while reactor temperature is small, long chains are not formed, the polymer becomes more uniform, and "fish-eye" problems may be reduced. Figure 4 shows experimental and simulation results obtained when the modifier is replaced by the same amount of an inhibitory species. In this case, it is assumed that inhibitor molecules are consumed by free radicals produced by initiator decomposition and that polymerization does not occur while the inhibitor is not completely consumed. It may be seen that results are very similar to the ones presented before, without the initial long polymer chains. One might think that it would take longer for inhibited reactions to be finished due to the existence of an induction period. Although the in-

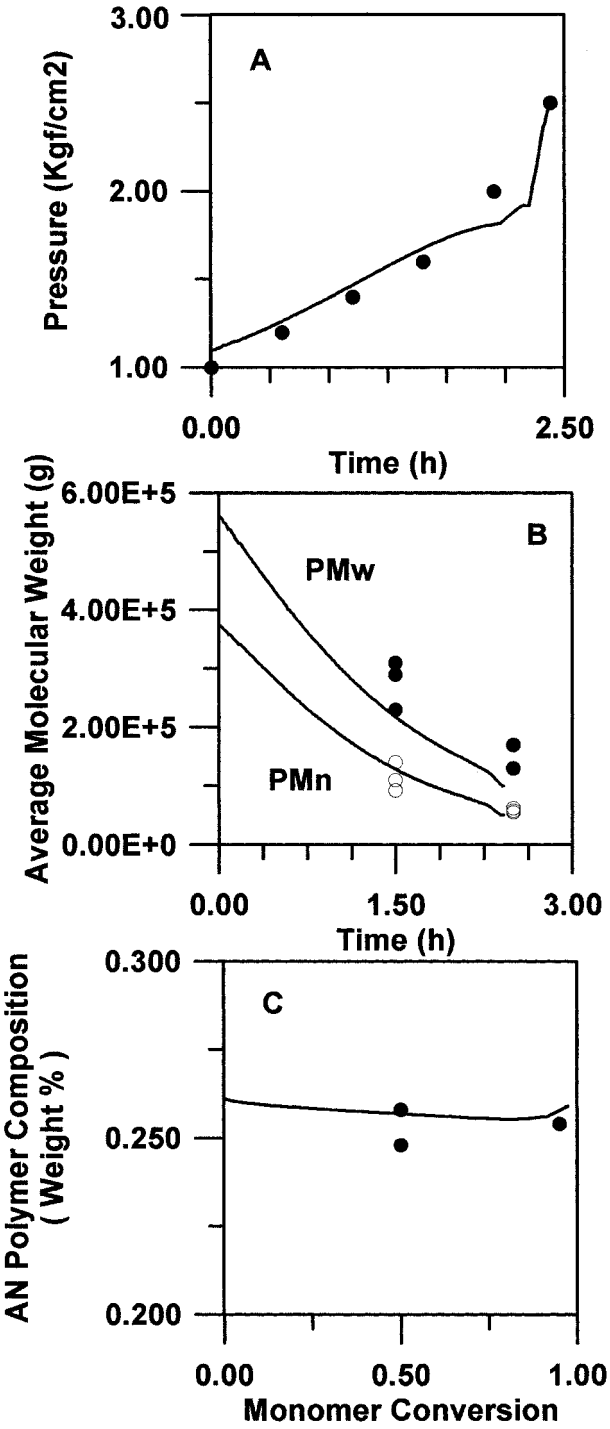

Figure 3 Comparison between experimental (●) and simulation (—) profiles obtained at actual operation conditions. (A) Pressure, (B) polymer average molecular weight, (C) polymer composition. Modifier model.

duction period is present, the delay is not significant because reaction begins at higher temperatures, so that reaction rates are higher than in the previous case.

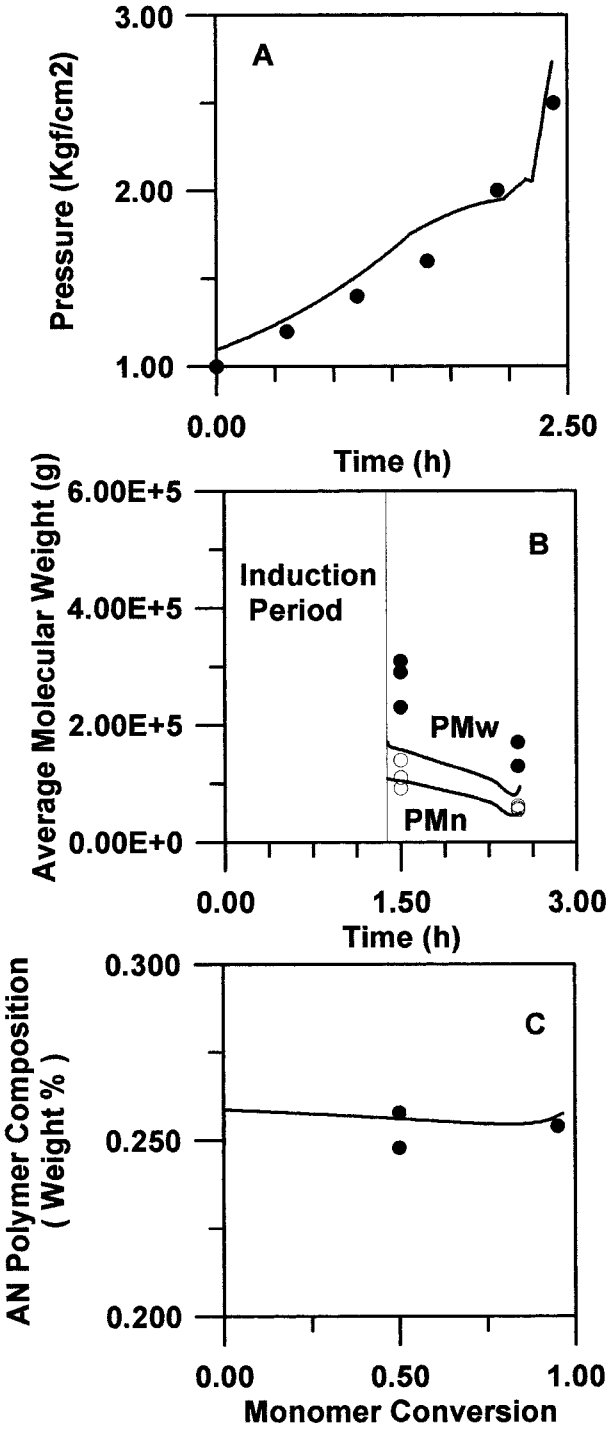

Figure 4 Comparison between experimental (●) and simulation (—) profiles obtained at actual operation conditions. (A) Pressure, (B) polymer average molecular weight, (C) polymer composition. Inhibition model.

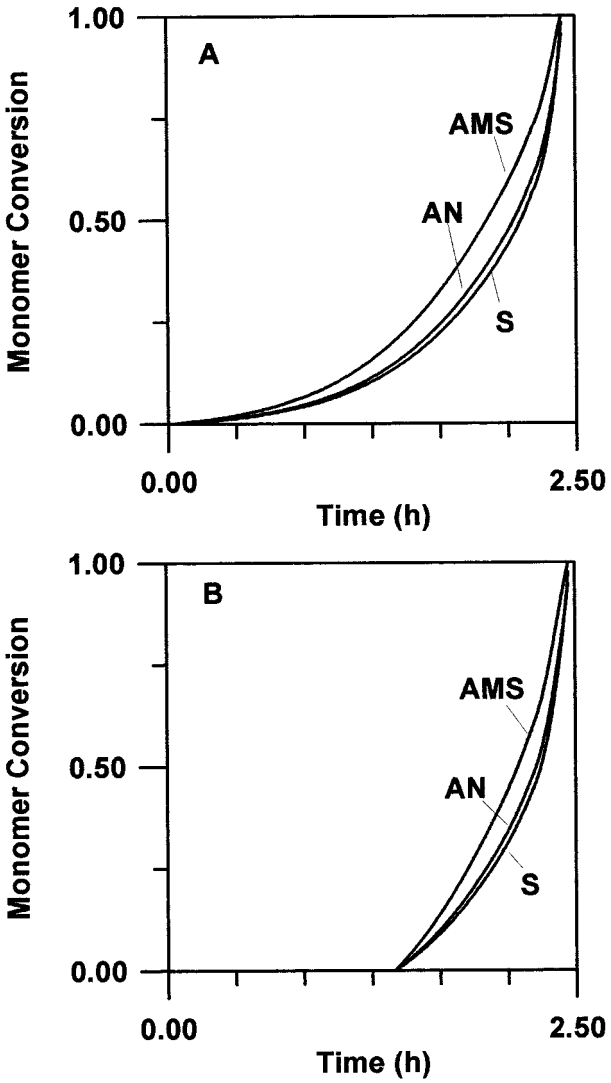

Figure 5 Individual monomer conversion profiles obtained through simulation at actual operation conditions. (A) Modifier model; (B) inhibition model.

Simulations

Based on the previous discussion, it is seen that the model is able to capture the most important features of the polymerization reactor. The behavior of other variables, which have not been verified experimentally, are now presented.

Figure 5 shows individual monomer conversion profiles. It is interesting to observe that AMS is consumed much faster than the other monomers, in spite of its much lower propagation constants. This is due to the reactivity ratios, as according to Table II radicals cross-propagate to AMS at higher rates than to the other monomers. Figure 6 shows, however, that AMS causes the decrease of the global polymerization rates and an increase

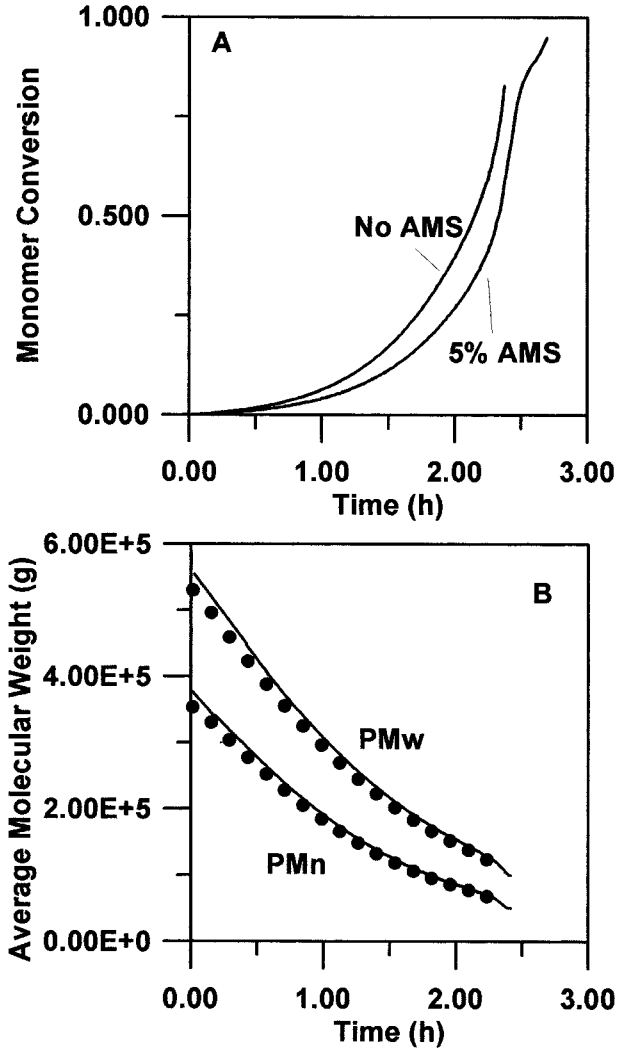

Figure 6 Effect of AMS on the reaction operation. Modifier model. (A) Monomer conversion; (B) polymer average molecular weight. No AMS feed (●) and 5% weight AMS feed (—).

of the reaction batch time. This is caused by the smaller propagation constants of AMS, as shown in Table II. As discussed by Rudin and Chiang,[31] however, the AMS termination constant may be 30 times larger than the styrene termination constant, instead of the value presented in Table II. Detailed sensitivity analysis carried out by Cavalcanti[42] showed, however, that increasing the termination constant of AMS by a factor of 30 would not lead to any significant change of the results presented. In spite of the smaller propagation rates, Figure 6 also shows that feeding small amounts of AMS does not cause any significant change of the molecular weight distribution. However, it allows the increase of the global monomer conversion by retarding the gel effect and the vitrification of the polymer beads. This is particularly important, because it contributes to the reduction of final residual monomer in the resin.

Although a depolymerization step was not included in the kinetic mechanism, AMS homopolymerization is strongly reversible at the reaction temperatures analyzed. This can also be used to explain the decrease of polymerization rates and average molecular weights when small amounts of AMS are added to the system, as AMS will not homopolymerize appreciably. However, cross-propagations are not expected to be affected.

An interesting point regards the control of the molecular weight distribution by adding small amounts of inhibitors to the reaction environment. Figure 7 shows that this may be effectively done if the reactor temperature varies along the batch. Figure 7 shows that increasing the initial inhibitor concentration causes a decrease of polymer average molecular weight, as reaction begins at higher temperatures. It seems that this possibility has been overlooked in the past. Most times industrial reactions are obliged to follow a temperature program due to operation constraints, so that final polymer resins are very heterogeneous. Inhibitors may be used to control the initial temperature of the batch, therefore allowing a better control of polymer properties. Figure 8 shows profiles obtained when similar amounts of modifier and inhibitor are used in different batches. It may be observed that, in spite of the slightly larger batch time, polymer obtained with the addition of inhibitor to the initial feed stream is much more

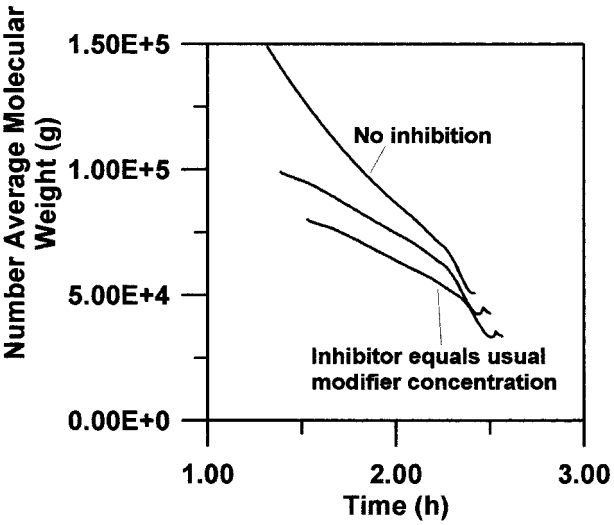

Figure 7 Polymer average molecular weight profiles obtained with different inhibitor concentrations. Inhibition model.

homogeneous than the polymer obtained when the same reaction is carried out in the presence of modifier.

Figure 9 shows that final acrylonitrile concentration in the aqueous phase may be > 1000 ppm at the end of the batch, which justifies careful water treatment before disposal. Figure 10 shows that the percentage of AN–AN bonds in the polymer chains is $\sim 1.8\%$ and is essentially constant throughout the batch. It is believed that AN–AN bonds cause the loss of transparency of the final resin, so that the computation of the AN–AN bonds may give us information about the optical properties of the final polymer produced. Results show that the optical properties of the resin are very homogeneous at the conditions analyzed.

OPTIMIZATION

In order to optimize the reactor operation, a profit function is defined as:

$$P\$ = Mas_{pol} * \$_{pol} - Cost_{bat} 24/t_{bat} \quad (1)$$

where

$$Cost_{bat} = Mas_1 * \$_1 + Mas_2 * \$_2 + Mas_3 * \$_3 + Mas_I * \$_I + Mas_L * \$_L + Mas_{pol} * \$_{util} + \$_{others} \quad (2)$$

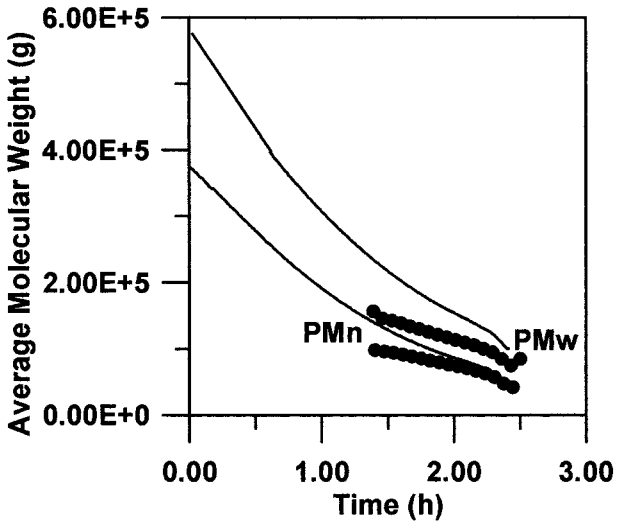

Figure 8 Polymer average molecular weight simulation profiles obtained when similar amounts of either modifier or inhibitor is added to the initial feed stream. (●) Inhibitor feed, (—) modifier feed.

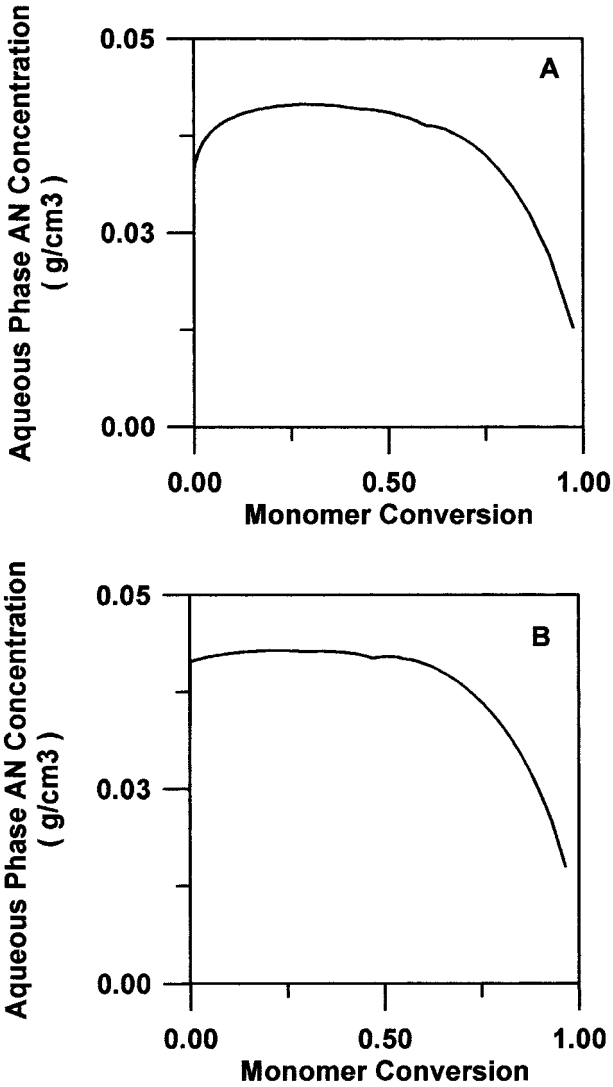

Figure 9 Acrylonitrile concentration in the aqueous phase. (A) Modifier model, (B) inhibition model.

and it is assumed that the utilities cost are proportional to the amount of polymer produced. Besides, the total batch time may be written as:

$$t_{bat} = t_{reaction} + t_{charge} + t_{discharge} + t_{cure} + t_{dead} \quad (3)$$

so that reaction time is only a fraction of the total batch. In all simulations, reaction was considered to be finished when either the initiator concentration had been completely consumed (the initiator concentration was $< 1 \times 10^{-10}$ gmol/L) or the free volume had fallen below the minimum critical value. When any of these two conditions are reached, reaction stops.

The optimization problem was also subject to some inequality constraints, to guarantee the

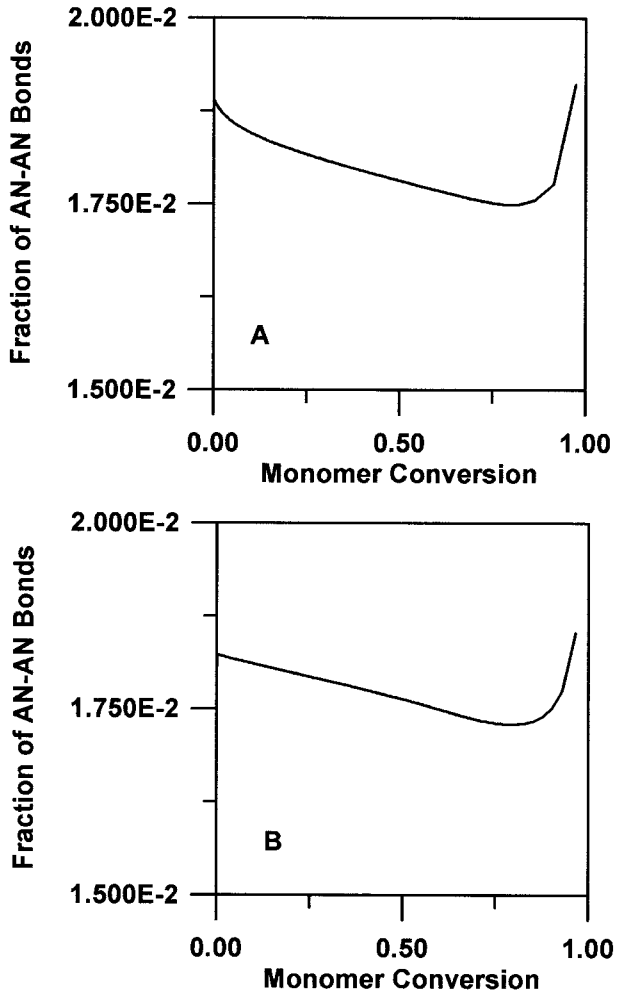

Figure 10 Fraction of AN–AN bonds in the polymer chains. (A) Modifier model; (B) inhibition model.

safety of the process operation and to assure the quality of the final polymer resin. Inequalities were defined as:

$$4 \times 10^4 \leq PM_n \leq 8 \times 10^4 \text{ g/gmol} \quad (4)$$

$$1 \times 10^5 \leq PM_w \leq 2 \times 10^5 \text{ g/gmol} \quad (5)$$

$$1.5 \leq PD \leq 3 \quad (6)$$

$$TRM \leq 8000 \text{ ppm} \quad (7)$$

$$P \leq 7 \text{ kgf/cm}^2 \quad (8)$$

The first problem analyzed regarded the optimization of the initial amount of initiator added to the polymerization reactor at usual plant operation conditions. Figure 11 shows how normalized profits depend on the initial initiator concentration for both uninhibited and inhibited polymerizations. It is important to notice that the normalized profit is obtained by dividing profits obtained through simulation by actual profits obtained after attaining maximum profit values at the plant site with the use of an evolutionary operation procedure. It can be observed that both model and actual data agree extremely well in the two cases. It is also interesting to observe that, as the initiator concentration increases, profits become relatively insensitive to changes of the initial initiator concentration. It must also be noticed that optimum initiator concentration does not depend on whether inhibited or uninhibited polymerization is being carried out. As actual profits are similar in both cases, optimum profits are also similar.

The second problem analyzed regarded the op-

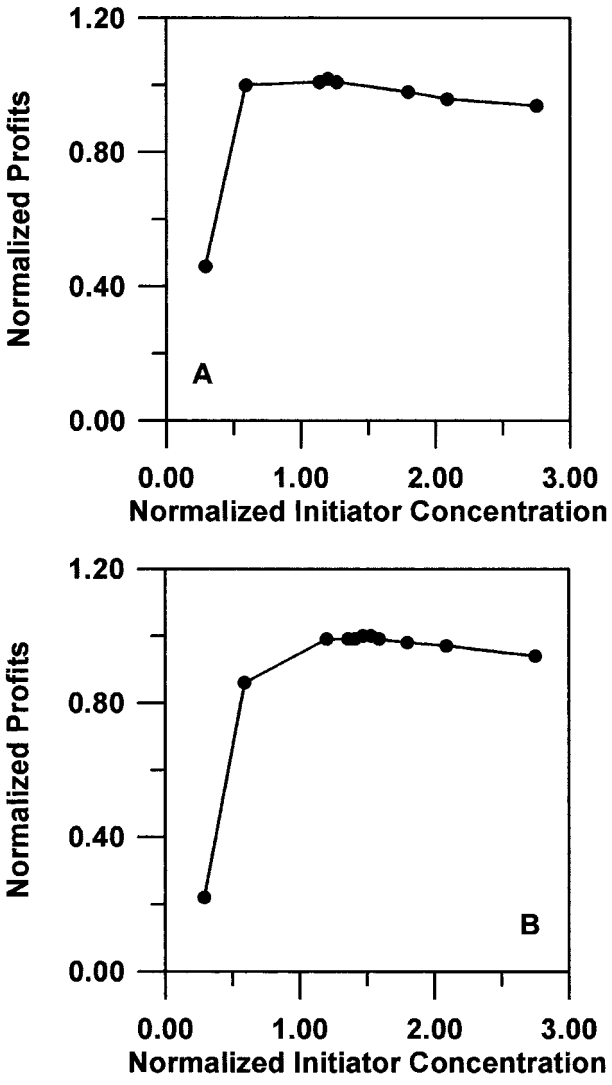

Figure 11 Normalized profits as a function of initial initiator concentration, optimization problem 1. (A) Modifier model, (B) inhibition model.

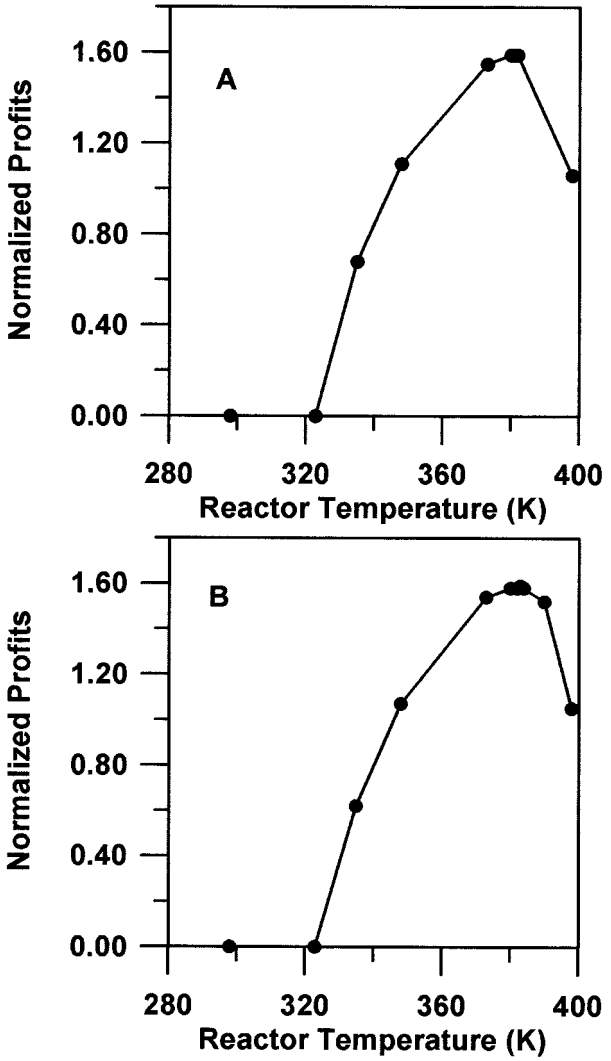

Figure 12 Normalized profits as a function of temperature, optimization problem 2. (A) Modifier model, (B) inhibition model.

timization of the reactor temperature at isothermal reaction conditions, keeping all other process conditions at usual plant values. Results are shown in Figure 12 for both uninhibited and inhibited polymerizations. It may be seen once more that the inhibited and uninhibited process operation strategies are alike. However, in this case, Figure 12 shows that a significant increase of plant profits may be possible. Figure 13 shows the experimental value of the heat transfer coefficient (U), measured at the plant site, and the calculated values of U that would be necessary to keep the reaction at isothermal condition when the jacket temperature is assumed to be the temperature of either the hot vapor or the cold water available at the plant site. Figure 13 shows that the optimum isothermal condition is not feasible and that the reaction would run out of control when $\sim$ 80% conversions were reached. Similar results were obtained in all isothermal simulations, as had already been observed by Secchi, Lima, and Pinto.[43] Therefore, the reaction cannot be carried out isothermally and the jacket temperature profile has to be optimized, subject to the experimental U constraint. It may be said, though, that profits may be significantly increased if the heat transfer conditions are improved.

The third problem analyzed regarded the optimization of the jacket temperature profile, keeping all other operation variables at usual plant values. As shown by Secchi, Lima, and Pinto[43] simulated optimum temperature profiles are frequently noisy and unfeasible. To avoid spurious results, additional temperature constraints were defined:

$$313 \leq T_c \leq 423 \text{ K} \qquad (9)$$

Besides, it was also assumed that the jacket temperature had to follow a linear or a parabolic control law, which can easily be implented at the plant site. In this case, optimizing the jacket profile is the same as optimizing a few control law parameters.

Figure 14 shows optimum jacket temperature and optimum simulated and experimental reactor temperature profiles for the parabolic control law case. Results obtained with the linear control law are very similar. It may be observed that optimum simulation and experimental results agree ex-

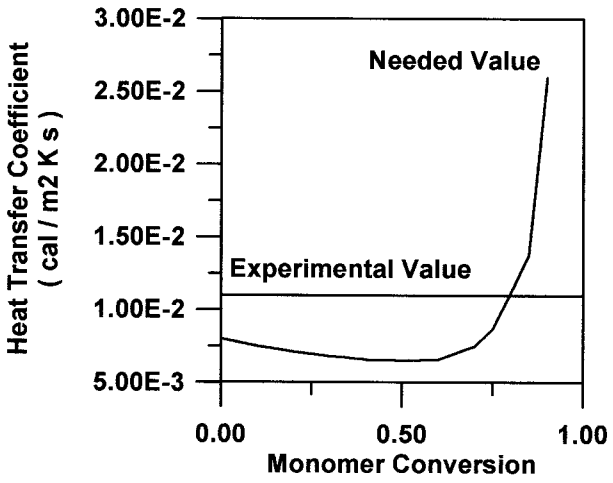

Figure 13 Heat transfer coefficients for optimum operation, optimization problem 2. Modifier model.

tremely well, no matter which technique is used to allow the control of the average polymer molecular weight. The final 1.5 h of the experimental reactor temperature profile should not be considered for comparison, as no reaction occurs during this time. Optimum normalized profits are equal to 1.08 and 0.99 in the uninhibited and inhibited reactions, respectively, which confirms the fact that the plant is already at optimum operation conditions, due to the experimental evolutionary operation procedure. The additional 8% profit gain that is predicted by the simulation, however, may be hard to get, as shown in Figure 15. Figure 15 shows reactor responses when one of the control law parameters is perturbed by $< 1\%$. It may be seen that a small increase of the control law parameter causes reactor temperature to increase much faster than in the optimum case, while a decrease of the control law parameter leads reaction to extinction. In the first case, normalized profits decrease to 1.00, while in the second case the operation leads to a no-profit situation. Profits are so sensitive to temperature profiles, that experimental results obtained may be regarded as excellent. Figure 16 shows results obtained when both initial initiator concentration and jacket temperature profiles are optimized simultaneously. In this case, simulation shows that profits may be increased by 17%, although results become even more sensitive to reaction operation conditions.

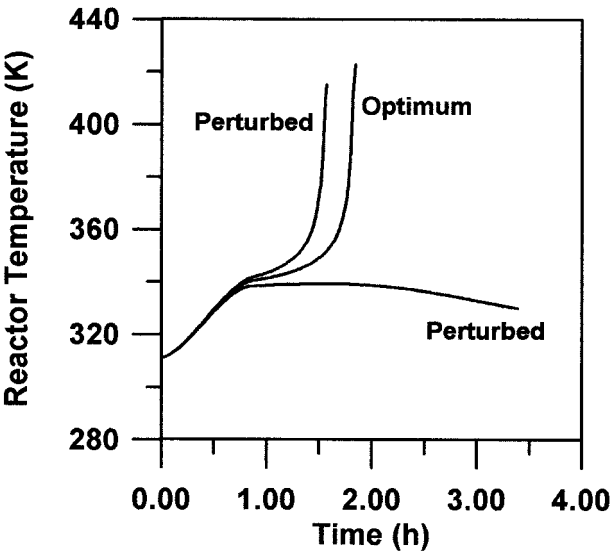

Figure 15 Perturbed temperature profiles, optimization problem 3. Modifier model.

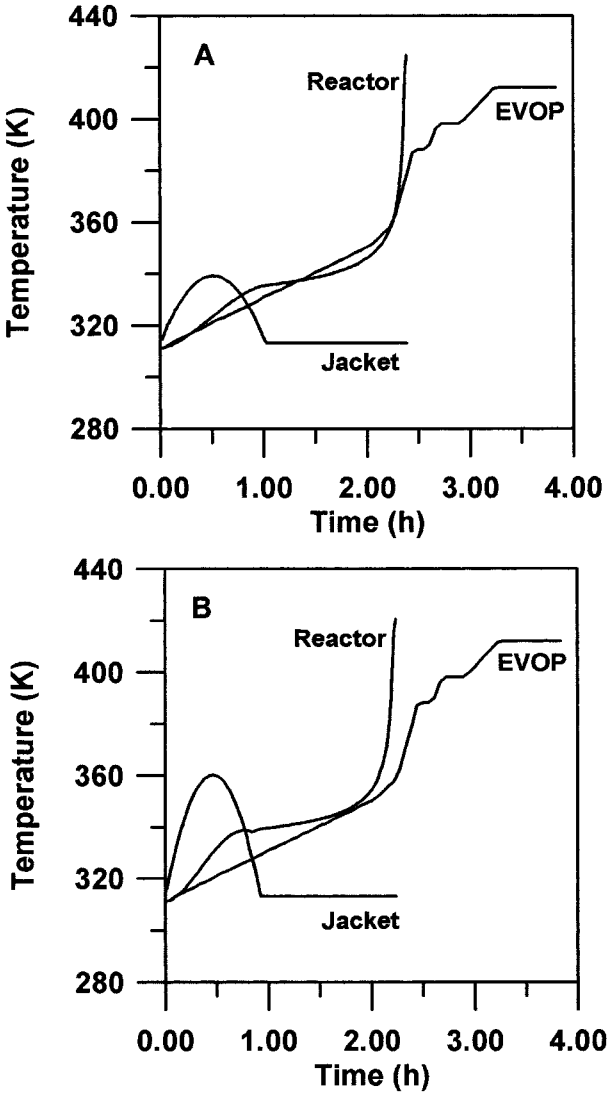

Figure 14 Optimum temperature profiles, optimization problem 3. (A) Modifier model, (B) inhibition model.

It is well known that polymerization reactions may present complex dynamic behaviors, which includes ignition–extinction phenomena.[44] As shown by Figures 15 and 16, the profit function sensitivity to changes of the operation parameters is due to the fact that the optimum operation conditions are placed at the border which separates regions of ignited and extinguished operation. To our knowledge, it is the first time that it is shown that the optimum operation point of a polymerization reactor may be placed at such an unstable condition. Secchi, Lima, and Pinto[43] had already pointed out that optimum operation conditions very frequently violate important process constraints, so that optimum conditions and process constraints must always be analyzed before final acceptance of optimum simulation results. In this case, no process constraint is violated (not even reached) and, in spite of that, the simulated opti-

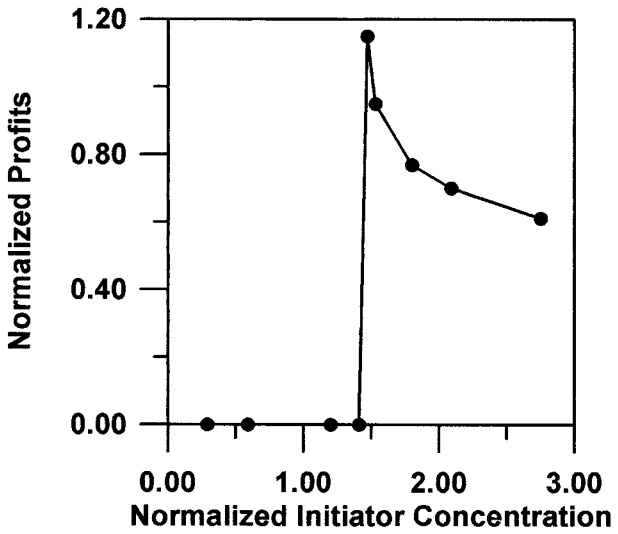

Figure 16 Normalized profits as a function of initial initiator concentration, optimization problem 4. Modifier model.

mum profile is not feasible either, given the huge sensitivity to the operation conditions. However, the implementation of an experimental evolutionary operation procedure was able to place the plant operation conditions very close to the optimum.

CONCLUSIONS

A mathematical model was developed to describe the modified SAN terpolymerization, allowing the reproduction of experimental data obtained at the plant site. It was shown through simulation that the AMS causes a reduction of the final average polymer molecular weight and allows the increase of the global monomer conversion, which contributes to reduction of final residual monomer in the resin. It was also shown that inhibitors may be used successfully to allow the control of the polymer molecular weight distribution. The model was used to optimize the process operation and final simulation results obtained agreed extremely well with independent experimental results obtained through the application of evolutionary optimization procedures. According to the simulations, optimal operation conditions are extremely sensitive to process parameters and may be placed at unstable conditions, so that the actual implementation of optimal operation conditions may be unfeasible.

The authors thank CNPq (Conselho Nacional de Desenvolvimento Científico e Tecnológico) for supporting this work, and Nitriflex Resinas for providing plant data and technical advice.

APPENDIX

Model Equations

In order to write the model equations, the following basic assumptions were made:

- Reactions are irreversible
- Polymerization follows the classical ultimate free-radical mechanism (Table I)
- The quasi-steady-state assumption is valid for radicals
- Kinetic constants do not depend on chain size
- Initiators, inhibitors, and chain transfer agents are not soluble in the aqueous phase
- Initiation efficiency does not depend on composition
- Individual phases are homogeneous and perfectly mixed
- Phases are in thermodynamic equilibrium
- Monomer activities in the organic phase follow the Flory–Huggins equation
- The vapor phase behaves as an ideal gas

In this case, the following equations may be written:

Monomer 1 Mass Balance

$$\frac{d(M_1^{\mathrm{I}}V^{\mathrm{I}})}{dt} + \frac{d(M_1^{\mathrm{II}}V^{\mathrm{II}})}{dt} = u_a M_{1a} - u_r\left(\frac{M_1^{\mathrm{I}}V^{\mathrm{I}} + M_1^{\mathrm{II}}V^{\mathrm{II}}}{V^{\mathrm{I}} + V^{\mathrm{II}}}\right) - k_s M_1^{\mathrm{II}^3} - k_{i\,1}[R\cdot] \times M_1^{\mathrm{II}}V^{\mathrm{II}} - (kp_{11} + kf_{11})P_0 M_1^{\mathrm{II}}V^{\mathrm{II}} - (kp_{21} + kf_{21})Q_0 M_1^{\mathrm{II}}V^{\mathrm{II}} - (kp_{31} + kf_{31})W_0 M_1^{\mathrm{II}}V^{\mathrm{II}} - kx_1[X\cdot]M_1^{\mathrm{II}}V^{\mathrm{II}} \quad (A.1)$$

Monomer 2 Mass Balance

$$\frac{d(M_2^{\mathrm{I}}V^{\mathrm{I}})}{dt} + \frac{d(M_2^{\mathrm{II}}V^{\mathrm{II}})}{dt} = u_a M_{2a} - u_r\left(\frac{M_2^{\mathrm{I}}V^{\mathrm{I}} + M_2^{\mathrm{II}}V^{\mathrm{II}}}{V^{\mathrm{I}} + V^{\mathrm{II}}}\right) - k_{i\,2}[R\cdot]M_2^{\mathrm{II}}V^{\mathrm{II}}$$

$$- (kp_{12} + kf_{12})P_0M_2^{II}V^{II} - (kp_{22} + kf_{22})Q_0M_2^{II}V^{II} - (kp_{32} + kf_{32})W_0M_2^{II}V^{II} - kx_2[X\cdot]M_2^{II}V^{II} \quad (A.2)$$

Monomer 3 Mass Balance

$$\frac{d(M_3^{I}V^{I})}{dt} + \frac{d(M_3^{II}V^{II})}{dt} = u_aM_{3a} - u_r\left(\frac{M_3^{I}V^{I} + M_3^{II}V^{II}}{V^{I} + V^{II}}\right) - k_{i3}[R\cdot]M_3^{II}V^{II} - (kp_{13} + kf_{13})P_0M_3^{II}V^{II} - (kp_{23} + kf_{23})Q_0M_3^{II}V^{II} - (kp_{33} + kf_{33})W_0M_3^{II}V^{II} - \mathrm{kx}_3[X\cdot]M_3^{II}V^{II} \quad (A.3)$$

where

$$P_0 = \sum_{n=0}^{\infty}\sum_{m=0}^{\infty}\sum_{l=0}^{\infty}P_{nml};\ Q_0 = \sum_{n=0}^{\infty}\sum_{m=0}^{\infty}\sum_{l=0}^{\infty}Q_{nml};\ W_0 = \sum_{n=0}^{\infty}\sum_{m=0}^{\infty}\sum_{l=0}^{\infty}W_{nml} \quad (A.4)$$

Initiator 1 Mass Balance

$$\frac{d(V^{II}I_1)}{dt} = u_aI_{1a} - u_r\left(\frac{V^{II}}{V^{I} + V^{II}}\right)I_1 - k_{D1}I_1V^{II} \quad (A.5)$$

Initiator 2 Mass Balance

$$\frac{d(V^{II}I_2)}{dt} = u_aI_{2a} - u_r\left(\frac{V^{II}}{V^{I} + V^{II}}\right)I_2 - k_{D2}I_2V^{II} \quad (A.6)$$

Chain Transfer Agent Mass Balance

$$\frac{d(V^{II}L)}{dt} = u_aL_a - u_r\left(\frac{V^{II}}{V^{I} + V^{II}}\right)L - kfl_1LP_0V^{II} - kfl_2LQ_0V^{II} - kfl_3LW_0V^{II} \quad (A.7)$$

Primary Radical Mass Balance

$$0 = 2f_1k_{D1}I_1V^{II} + 2f_2k_{D2}I_2V^{II} - ki_1[R\cdot]M_1^{II}V^{II} - ki_2[R\cdot]M_2^{II}V^{II} - ki_3[R\cdot]M_3^{II}V^{II} \quad (A.8)$$

$$k_{i1}[R\cdot] = k_{i2}[R\cdot] = k_{i3}[R\cdot] = \frac{2f_1k_{D1}I_1 + 2f_2k_{D2}I_2}{M_1 + M_2 + M_3} \quad (A.9)$$

Chain Transfer Radical Mass Balance

$$0 = kfl_1LV^{II} + kfl_2LV^{II} + kfl_3LV^{II} - kx_1[X\cdot]M_1^{II}V^{II} - kx_2[X\cdot]M_2^{II}V^{II} - kx_3[X\cdot]M_3^{II}V^{II} \quad (A.10)$$

$$kx_1[X\cdot] = kx_2[X\cdot] = kx_3[X\cdot] = \frac{kfl_1L + kfl_2L + kfl_3L}{M_1 + M_2 + M_3} \quad (A.11)$$

Polymer Radical ($\mathbf{P}_{1,0,0}$) Mass Balance

$$0 = k_sM_1^{II3}V^{II} + k_{i1}[R\cdot]M_1^{II}V^{II} + (kf_{11}P_0 + kf_{21}Q_0 + kf_{31}W_0)M_1^{II}V^{II} + k_{X1}[X\cdot]M_1^{II}V^{II} - [(kp_{11} + kf_{11})M_1^{II} + (kp_{12} + kf_{12})M_2^{II} + (kp_{13} + kf_{13})M_3^{II} + (kc_{11} + kd_{11})P_0 + (kc_{12} + kd_{12})Q_0 + (kc_{13} + kd_{13})W_0 + kfl_1L]P_{1,0,0}V^{II} \quad (A.12)$$

Polymer Radical ($\mathbf{Q}_{0,1,0}$) Mass Balance

$$0 = k_{i2}[R\cdot]M_2^{II}V^{II} + (kf_{12}P_0 + kf_{22}Q_0 + kf_{32}W_0)M_2^{II}V^{II} + k_{X2}[X\cdot]M_2^{II}V^{II} - [(kp_{21} + kf_{21})M_1^{II} + (kp_{22} + kf_{22})M_2^{II} + (kp_{23} + kf_{23})M_3^{II} + (kc_{12} + kd_{12})P_0 + (kc_{22} + kd_{22})Q_0 + (kc_{23} + kd_{23})W_0 + kfl_2L]Q_{0,1,0}V^{II} \quad (A.13)$$

Polymer Radical ($\mathbf{W}_{0,0,1}$) Mass Balance

$$0 = k_{i3}[R\cdot]M_3^{II}V^{II} + (kf_{13}P_0 + kf_{23}Q_0 + kf_{33}W_0)M_3^{II}V^{II} + k_{X3}[X\cdot]M_3^{II}V^{II} - [(kp_{31} + kf_{31})M_1^{II} + (kp_{32} + kf_{32})M_2^{II} + (kp_{33} + kf_{33}) \times M_3^{II} + (kc_{13} + kd_{13})P_0 + (kc_{23} + kd_{23})Q_0 + (kc_{33} + kd_{33})W_0 + kfl_3L]W_{0,0,1}V^{II} \quad (A.14)$$

Polymer Radical ($P_{n,m,l}$) Mass Balance

$$0 = (kp_{11}P_{n-1,m,l} + kp_{21}Q_{n-1,m,l} + kp_{31}W_{n-1,m,l}) \times M_1^{II}V^{II} - [(kp_{11} + kf_{11})M_1^{II} + (kp_{12} + kf_{12})M_2^{II} + (kp_{13} + kf_{13}) \times M_3^{II} + (kc_{11} + kd_{11})P_0 + (kc_{12} + kd_{12})Q_0 + (kc_{13} + kd_{13})W_0 + kfl_1L]P_{n,m,l}V^{II} \quad (A.15)$$

Polymer Radical ($Q_{n,m,l}$) Mass Balance

$$0 = (kp_{12}P_{n,m-1,l} + kp_{22}Q_{n,m-1,l} + kp_{32}W_{n,m-1,l}) \times M_2^{II}V^{II} - [(kp_{21} + kf_{21})M_1^{II} + (kp_{22} + kf_{22})M_2^{II} + (kp_{23} + kf_{23}) \times M_3^{II} + (kc_{12} + kd_{12})P_0 + (kc_{22} + kd_{22})Q_0 + (kc_{23} + kd_{23})W_0 + kfl_2L]Q_{n,m,l}V^{II} \quad (A.16)$$

Polymer Radical ($W_{n,m,l}$) Mass Balance

$$0 = (kp_{13}P_{n,m,l-1} + kp_{23}Q_{n,m,l-1} + kp_{33}W_{n,m,l-1}) \times M_3^{II}V^{II} - [(kp_{31} + kf_{31})M_1^{II} + (kp_{32} + kf_{32})M_2^{II} + (kp_{33} + kf_{33}) \times M_3^{II} + (kc_{13} + kd_{13})P_0 + (kc_{23} + kd_{23})Q_0 + (kc_{33} + kd_{33})W_0 + kfl_3L]W_{n,m,l}V^{II} \quad (A.17)$$

Dead Polymer Chain ($\Lambda_{n,m,l}$) Mass Balance

$$\frac{d(V^{II}\Lambda_{n,m,l})}{dt} = \frac{1}{2}kc_{11}\sum_{r=0}^{n}\sum_{q=0}^{m}\sum_{z=0}^{l}P_{r,q,z}P_{n-r,m-q,l-z}V^{II} + kc_{12}\sum_{r=0}^{n}\sum_{q=0}^{m}\sum_{z=0}^{l}P_{r,q,z}Q_{n-r,m-q,l-z}V^{II} + \frac{1}{2}kc_{13}\sum_{r=0}^{n}\sum_{q=0}^{m}\sum_{z=0}^{l}P_{r,q,z}W_{n-r,m-q,l-z}V^{II} + \frac{1}{2}kc_{23}\sum_{r=0}^{n}\sum_{q=0}^{m}\sum_{z=0}^{l}Q_{r,q,z}Q_{n-r,m-q,l-z}V^{II} + \frac{1}{2}kc_{23}\sum_{r=0}^{n}\sum_{q=0}^{m}\sum_{z=0}^{l}Q_{r,q,z}W_{n-r,m-q,l-z}V^{II} + \frac{1}{2}kc_{33}\sum_{r=0}^{n}\sum_{q=0}^{m}\sum_{z=0}^{l}W_{r,q,z}W_{n-r,m-q,l-z}V^{II} + kd_{11}P_{n,m,l}P_0V^{II} + kd_{12} \times (P_{n,m,l}Q_0 + Q_{n,m,l}P_0)V^{II} + kd_{13}(P_{n,m,l}W_0 + W_{n,m,l}P_0)V^{II} + kd_{22}Q_{n,m,l}Q_0V^{II} + kd_{23} \times (Q_{n,m,l}W_0 + W_{n,m,l}Q_0)V^{II} + kd_{33}W_{n,m,l}W_0V^{II} + (kf_{11}M_1^{II} + kf_{12}M_2^{II} + kf_{13}M_3^{II} + kfl_1L) \times P_{n,m,l}V^{II} + (kf_{21}M_1^{II} + kf_{22}M_2^{II} + kf_{23}M_3^{II} + kfl_2L)Q_{n,m,l}V^{II} + (kf_{31}M_1^{II} + kf_{32}M_2^{II} + kf_{33}M_3^{II} + kfl_3L) \times W_{n,m,l}V^{II} - u_r\left(\frac{V^{II}}{V^{I} + V^{II}}\right)\Lambda_{n,m,l} \quad (A.18)$$

Water Mass Balance

$$\frac{d(V^{I}Wt)}{dt} = u_aWt_a - u_r\frac{V^{I}}{V^{I} + V^{II}}Wt \quad (A.19)$$

Global Mass Balance

$$\frac{d(MAS)}{dt} = u_a(M_{1a} + M_{2a} + M_{3a} + L_a + I_{1a} + I_{2a} + Wt_a) - u_r\left(\frac{V^{I}}{V^{I} + V^{II}}\right)\rho_m^{I} - u_r\left(\frac{V^{II}}{V^{I} + V^{II}}\right)\rho_m^{II} \quad (A.20)$$

Balance of AN–AN Bonds

$$\frac{d(V^{II}\Gamma)}{dt} = kp_{22}Q_0M_2^{II}V^{II} + kc_{22}Q_0Q_0V^{II} - u_r\left(\frac{V^{II}}{V^{I} + V^{II}}\right)\Gamma \quad (A.21)$$

Energy Balance

$$(\rho_m^{I}C_p^{I}V^{I} + \rho_m^{II}C_p^{II}V^{II})\frac{dT}{dt} = u_a\rho_aC_{pa}(T_a - T) - UA(T - T_c) + V^{II}\Delta H_rR \quad (A.22)$$

where

$$R = [(kp_{11} + kf_{11})P_0 + (kp_{21} + kf_{21})Q_0 + (kp_{31} + kf_{31})W_0]M_1^{II} + [(kp_{12} + kf_{12})P_0 + (kp_{22} + kf_{22})Q_0 + (kp_{32} + kf_{32})W_0]$$

$$\times M_2^{II} + [(kp_{13} + kf_{13})P_0 + (kp_{23} + kf_{23})Q_0 + (kp_{33} + kf_{33})W_0]M_3^{II} \quad (A.23)$$

Total Mass Definition

$$MAS = V^I\rho_m^I + V^{II}\rho_m^{II} \quad (A.24)$$

Thermodynamic Equilibrium Constraints

$$M_1^I = K_1 M_1^{II} \quad (A.25)$$

$$M_3^I = K_3 M_3^{II} \quad (A.26)$$

$$\frac{\theta_1^{II}\omega_2^{II}}{\rho_2 - \theta_2^{II}\omega_2^{II}} \exp\left[\left(\frac{1 - \theta_1^{II}\omega_2^{II}}{\rho_2 - \theta_2^{II}\omega_2^{II}}\right)\left(1 - \frac{\vartheta_2}{\vartheta_1}\right)\right] = \phi_2^{II}\exp\left[\phi_1^{II}\left(1 - \frac{\vartheta_2}{\vartheta_1}\right) + \phi_p + \chi\phi_1^{II}\phi_p\left(1 - \frac{\vartheta_2}{\vartheta_1}\right) + \chi\phi_p^2\right] \quad (A.27)$$

where

$$\theta_1^{II} = \frac{0.8PM_2\rho_{wt}\rho_1}{0.14PM_{wt}\rho_2 f(T)} \quad (A.28)$$

$$\theta_2^{II} = \frac{(1.8\rho_2 - 0.8\rho_1)PM_2\rho_{wt}}{0.14PM_{wt}\rho_2 f(T)} \quad (A.29)$$

$$\omega_2^I = \frac{M_2^I V^I PM_{wt}}{MAS_{wt}} \quad (A.30)$$

$$f(T) = \frac{(T - 273) + 50}{100} \quad (A.31)$$

Composition Constraint

$$\phi_1 + \phi_2 + \phi_3 + \phi_{Wt} = 1 \quad (A.32)$$

System Pressure

$$P = P_{SAT}^I + P_{SAT}^{II} + P_{N2} \quad (A.33)$$

where

$$P_{SAT}^I = P_{SAT_{Wt}}$$

$$P_{SAT}^{II} = P_{SAT_1}\phi_1^{II}\exp[(1 - \phi_{pol}) + \chi_1\phi_{pol}^2] + P_{SAT_2}\phi_2^{II}\exp[(1 - \phi_{pol}) + \chi_2\phi_{pol}^2] + P_{SAT_3}\phi_3^{II}\exp[(1 - \phi_{pol}) + \chi_3\phi_{pol}^2] \quad (A.34)$$

Moment Balances

The well-known method of moments was used to describe the first averages of the molecular weight distribution for both radical and dead polymer chains. The moments are defined as:

$$p_{i,j,k} = \sum_{n=0}^{\infty}\sum_{m=0}^{\infty}\sum_{l=0}^{\infty} n^i m^j l^k P_{n,m,l} \qquad i, j, k = 0, 1, 2, \cdots \quad (A.35)$$

$$q_{i,j,k} = \sum_{n=0}^{\infty}\sum_{m=0}^{\infty}\sum_{l=0}^{\infty} n^i m^j l^k Q_{n,m,l} \qquad i, j, k = 0, 1, 2, \cdots \quad (A.36)$$

$$w_{i,j,k} = \sum_{n=0}^{\infty}\sum_{m=0}^{\infty}\sum_{l=0}^{\infty} n^i m^j l^k W_{n,m,l} \qquad i, j, k = 0, 1, 2, \cdots \quad (A.37)$$

$$\mu_{i,j,k} = \sum_{n=0}^{\infty}\sum_{m=0}^{\infty}\sum_{l=0}^{\infty} n^i m^j l^k \Lambda_{n,m,l} \qquad i, j, k = 0, 1, 2, \cdots \quad (A.38)$$

The moment balances are presented by Cavalcanti[42] and will not be presented here for lack of space.

Monomer Conversion

$$X_1 = \frac{\mu_{100}}{\mu_{100} + M_1^{II}} \quad (A.39)$$

$$X_2 = \frac{\mu_{010}}{\mu_{010} + M_2^{II}} \quad (A.40)$$

$$X_3 = \frac{\mu_{001}}{\mu_{001} + M_3^{II}} \quad (A.41)$$

$$X_{POL} = \frac{\mu_1}{\mu_1 + M_1^{II} + M_2^{II} + M_3^{II}} \quad (A.42)$$

Composition of Polymer Chains

$$IM_1 = \frac{\mu_{100}PM_1}{\mu_{100}PM_1 + \mu_{010}PM_2 + \mu_{001}PM_3} \quad (A.43)$$

$$IM_2 = \frac{\mu_{010}PM_2}{\mu_{100}PM_1 + \mu_{001}PM_2 + \mu_{001}PM_3} \quad (A.44)$$

$$IM_3 = \frac{\mu_{001} PM_3}{\mu_{100} PM_1 + \mu_{010} PM_2 + \mu_{001} PM_3} \quad \text{(A.45)}$$

Polymer Number Average Molecular Weight

$$PM_n = \frac{\mu_{100} PM_1 + \mu_{010} PM_2 + \mu_{001} PM_3}{\mu_0} \quad \text{(A.46)}$$

Polymer Weight Average Molecular Weight

$$PM_w = \frac{\begin{array}{c}\mu_{200} PM_1^2 + \mu_{020} PM_2^2 \\ + \mu_{002} PM_3^2 + 2\mu_{110} PM_1 PM_2 \\ + 2\mu_{101} PM_1 PM_3 + 2\mu_{011} PM_2 PM_3\end{array}}{\mu_{100} PM_1 + \mu_{010} PM_2 + \mu_{001} PM_3} \quad \text{(A.47)}$$

Polydispersity

$$PD = \frac{PM_w}{PM_n} = \frac{\begin{array}{c}(\mu_{200} PM_1^2 + \mu_{020} PM_2^2 \\ + \mu_{002} PM_3^2 + 2\mu_{110} PM_1 PM_2 \\ + 2\mu_{101} PM_1 PM_3 + 2\mu_{011} 2PM_2 PM_3)\mu_0\end{array}}{(\mu_{100} PM_1 + \mu_{010} PM_2 + \mu_{001} PM_3)^2} \quad \text{(A.48)}$$

AN–AN Bond Fraction

$$\xi = \frac{\Gamma}{\mu_{100} + \mu_{010} + \mu_{001} - \mu_0} \quad \text{(A.49)}$$

Residual Monomer

$$TRM = \frac{MAS_1 + MAS_2 + MAS_3 - MAS_{POL}}{V^{\mathrm{I}} + V^{\mathrm{II}}} \quad \text{(A.50)}$$

Gel Effect Correlation

Termination and propagation constants were assumed to vary in accordance to the following equations, based on the Free Volume Theory:

$$kc_{ij} = kc_{ij0} \exp\left[A\left(\frac{1}{V_f} - \frac{1}{V_{fcr1}}\right)\right] \quad \text{(A.51)}$$

$$kp_{ij} = kp_{ij0} \exp\left[B\left(\frac{1}{V_f} - \frac{1}{V_{fcr2}}\right)\right] \quad \text{(A.52)}$$

$$V_f = \sum_{1,2,3,p} [0.025 + \alpha_i (T - T_{gi})]\phi_i \quad \text{(A.53)}$$

where A, B, and V_{fcr2} are equal to 0.32, 1.7, and 0.035, respectively. Other parameters are presented by Garcia-Rubio et al.[14]

Physical Properties

All physical parameters needed for simulation may be obtained in standard reference books[45,46] and are presented by Cavalcanti.[42]

NOMENCLATURE

A	heat transfer area
Cost	batch costs
C_p	specific heat capacity
f	initiator efficiency
I	initiator, initiator concentration
IM_i	mass fraction of species i in the final polymer
kc_{ij}	kinetic constant for termination by combination
kd_{ij}	kinetic constant for termination by disproportionation
k_{Di}	kinetic constant for initiator decomposition
kf_{ij}	kinetic constant for chain transfer to monomer
kfl_{ij}	kinetic constant for chain transfer to modifier
k_{ii}	kinetic constant for propagation to $R\cdot$
kp_{ij}	kinetic constant for propagation
k_s	kinetic constant for spontaneous styrene initiation
k_{xi}	kinetic constant for propagation to $X\cdot$
K	partition coefficient
L	chain transfer agent (modifier), chain transfer agent concentration
M_i	monomer i, concentration of monomer i
Mas_i	mass of species i
MAS	total mass
p_{ijk}	moment ijk of radicals P_{nml}
P	pressure
P_0	total concentration of radicals containing monomer 1 at the active end
P_{nml}	concentration of radicals with monomer 1 at the active site which contain n mers of monomer 1, m mers of monomer 2, and l mers of monomer 3
PD	polydispersity
PM_i	molecular weight of species i
PM_n	number average polymer molecular weight
PM_w	weight average polymer molecular weight
$P\$$	daily profits
q_{ijk}	moment ijk of radicals Q_{nml}

Q_0 total concentration of radicals containing monomer 2 at the active end
Q_{nml} concentration of radicals with monomer 2 at the active site which contain n mers of monomer 1, m mers of monomer 2, and l mers of monomer 3
r_{ij} reactivity ratio
R global reaction rate
$R\cdot$ initiator fragment
t time
T temperature
TRM total residual monomer
u volumetric flow rate
U global heat transfer coefficient
V volume
V_f free volume
$X\cdot$ chain transfer fragment
X_i conversion of monomer i
w_{ijk} moment ijk of radicals W_{nml}
W_0 total concentration of radicals containing monomer 3 at the active end
W_{nml} concentration of radicals with monomer 3 at the active site, which contain n mers of monomer 1, m mers of monomer 2, and l mers of monomer 3
Wt water, water concentration

Greek

χ Flory–Huggins interaction parameter
ΔH_r heat of polymerization
ϕ volume fraction
Γ concentration of AN–AN bonds
φ_{ij} cross-termination constant
Λ_{nml} concentration of dead polymer chains containing n mers of monomer 1, m mers of monomer 2, and l mers of monomer 3
μ_m sum of all moments ijk of radicals Λ_{nml} where $m = i + j + k$
μ_{ijk} moment ijk of radicals Λ_{nml}
ρ density

Symbols

$\$_i$ unit price of item i
$[\cdot]$ concentration of

Subscript

1 monomer 1 (styrene)
2 monomer 2 (acrylonitrile)
3 monomer 3 (α-methylstyrene)
a feed
bat batch
c jacket
cr critical value
I initiator
g glass transition
L chain transfer agent
m mixture
$N2$ inert atmosphere
p, pol polymer
r outlet
SAT saturation
$util$ utilities
Wt water

Superscript

I phase I (organic phase)
II phase II (aqueous phase)

REFERENCES

1. D. Savostianoff and E. R. Didier, *Caout. Plast.,* **734,** 45 (1994).
2. H. G. Yuan, G. Kalfas, and W. H. Ray, *Rev. Macromol. Chem. Phys.,* **31,** 215 (1991).
3. M. A. Villalobos, A. E. Hamielec, and P. E. Wood, *J. Appl. Polym. Sci.,* **50,** 327 (1993).
4. G. Maschio, T. Bello, and C. Scali, *Chem. Eng. Sci.,* **47,** 2609 (1992).
5. D. Bretelle and S. Macchietto, *Comp. Chem. Eng.,* **S,** S317 (1992).
6. C. G. Hagberg, *Polym. Mater. Sci. Eng.,* **58,** 614 (1988).
7. G. Kalfas and W. H. Ray, *Ind. Eng. Chem. Res.,* **32,** 1822 (1993).
8. G. Kalfas, H. Yuan, and W. H. Ray, *Ind. Eng. Chem. Res.,* **32,** 1831 (1993).
9. T. Myiata and F. Makashio, *Kogaku-Kogaku,* **37,** 607 (1973).
10. V. M. Belyaev, V. F. Kazanskaya, and S. G. Nikitina, *Int. Polym. Sci. Technol.,* **15,** 91 (1988).
11. G. Xiuchun, *Shiyou-Huagong,* **20,** 463 (1991).
12. D. H. Sebastian and J. A. Biesenberger, *Polym. Eng. Sci.,* **19,** 190 (1979).
13. K. S. Balaraman, B. D. Sarwade, and V. M. Nadkarni, *J. Polym. Sci., Polym. Lett.,* **21,** 739 (1983).
14. L. H. Garcia-Rubio, M. G. Lord, J. F. MacGregor, and A. E. Hamielec, *Polymer,* **26,** 2001 (1985).
15. D. Liu, A. B. Padias, and H. K. Hall, *Macromolecules,* **28,** 622 (1995).
16. Y. Hatate, T. Hano, T. Miyata, W. Sakai, and F. Nakashio, *Kogaku Kogaku,* **35,** 903 (1970).
17. Y. Hatate, T. A. Otake, A. Ikari, and F. Nakashio, *J. Chem. Eng. Japan,* **17,** 158 (1984).
18. B. N. Hendy, *J. Appl. Polym. Sci.,* **38,** 115 (1989).
19. T. Kikuta and S. Omi, *J. Chem. Eng. Japan,* **9,** 64 (1975).
20. C. C. Lin, W. Y. Chiu, and C. T. Wang, *J. Appl. Polym. Sci.,* **23,** 1203 (1979).

21. D. H. Sebastian and J. A. Biesenberger, *J. Macromol. Sci. Chem.,* **A15,** 553 (1981).
22. V. Dimonie, M. S. El Aaser, A. Klein, and J. W. Vanderhoff, *J. Polym. Sci. Chem.,* **22,** 2197 (1984).
23. S. Djekhaba, C. Graillat, and J. Guillot, *Eur. Polym. J.,* **22,** 729 (1986).
24. J. Guillot, *Makromol. Chem.,* **10/11,** 165 (1985).
25. J. Guillot, *New J. Chem.,* **11,** 787 (1987).
26. A. B. Deshpande, S. S. Dixit, L. C. Anand, and S. L. Kapur, *J. Polym. Sci. B,* **8,** 267 (1970).
27. V. G. Gandhi, S. Sivaram, and I. S. Bhardwaj, *J. Macromol. Sci. Chem.,* **A19,** 147 (1983).
28. G. Ham, *J. Polym. Sci.,* **19,** 183 (1960).
29. G. G. Lowry, *J. Polym. Sci.,* **42,** 463 (1960).
30. P. Wittmer, *ACS Polymer Preprints,* **11,** 367 (1970).
31. A. Rudin and S. S. M. Chiang, *J. Polym. Sci. Chem.,* **12,** 2235 (1974).
32. A. Rudin and M. C. Samanta, *J. Appl. Polym. Sci.,* **24,** 1665 (1979).
33. M. E. Souza, E. L. Lima, and J. C. Pinto, *Polym. Eng. Sci.,* **36,** 433 (1996).
34. Y. Soni and L. F. Albright, *J. Appl. Polym. Sci., Appl. Polym. Symp.,* **36,** 113 (1981).
35. L. F. Albright and Y. Soni, *J. Macromol. Sci. Chem.,* **A1,** 1065 (1982).
36. M. Tirrel and K. Gromley, *Chem. Eng. Sci.,* **36,** 367 (1981).
37. A. Tsoukas, M. Tirrel, and G. Stephanopoulos, *Chem. Eng. Sci.,* **37,** 1785 (1982).
38. J. N. Farber, *Polym. Eng. Sci.,* **26,** 499 (1986).
39. G. D. Cawthon and K. S. Knaebel, *Comp. Chem. Eng.,* **13,** 63 (1989).
40. K. Y. Choi, *J. Appl. Polym. Sci.,* **37,** 1429 (1989).
41. L. R. Petzold, *DDASSL Code. Version 1989,* Lawrence Livermore National Laboratory, 1989.
42. M. J. R. Cavalcanti, M.Sc. Thesis, PEQ/COPPE, 1995.
43. A. R. Secchi, E. L. Lima, and J. C. Pinto, *Polym. Eng. Sci.,* **30,** 1209 (1990).
44. J. C. Pinto and W. H. Ray, *Chem. Eng. Sci.,* **50,** 715 (1995).
45. J. M. Prausnitz, R. C. Reid, and B. E. Poling, *The Properties of Gases and Liquids,* McGraw–Hill, New York, 1988.
46. J. Brandrup and E. H. Immergut, *Polymer Handbook,* Wiley, New York, 1975.
47. A. W. Hui and A. E. Hamielec, *J. Appl. Polym. Sci.,* **16,** 749 (1972).